

Positron emission tomography probe demonstrates a striking concentration of ribose salvage in the liver

Peter M. Clark^{a,1}, Graciela Flores^{b,c}, Nikolai M. Evdokimov^{b,d}, Melissa N. McCracken^b, Timothy Chai^a, Evan Nair-Gill^b, Fiona O'Mahony^e, Simon W. Beaven^e, Kym F. Faulf^{f,g}, Michael E. Phelps^{b,c,1}, Michael E. Jung^d, and Owen N. Witte^{a,b,h,i,1}

Departments of ^aMicrobiology, Immunology, and Molecular Genetics, ^bMolecular and Medical Pharmacology, ^dChemistry and Biochemistry, and ^gPsychiatry and Biobehavioral Sciences, ^cCrump Institute for Molecular Imaging, ^eDivision of Digestive Diseases, ^fPasarow Mass Spectrometry Laboratory, Semel Institute for Neuroscience and Human Behavior, ^hEli and Edythe Broad Center of Regenerative Medicine and Stem Cell Research, and ⁱHoward Hughes Medical Institute, David Geffen School of Medicine, University of California, Los Angeles, CA 90095

Contributed by Michael E. Phelps, June 5, 2014 (sent for review March 10, 2014)

PET is a powerful technique for quantifying and visualizing biochemical pathways in vivo. Here, we develop and validate a novel PET probe, [¹⁸F]-2-deoxy-2-fluoroarabino ([¹⁸F]DFA), for in vivo imaging of ribose salvage. DFA mimics ribose in vivo and accumulates in cells following phosphorylation by ribokinase and further metabolism by transketolase. We use [¹⁸F]DFA to show that ribose preferentially accumulates in the liver, suggesting a striking tissue specificity for ribose metabolism. We demonstrate that solute carrier family 2, member 2 (also known as GLUT2), a glucose transporter expressed in the liver, is one ribose transporter, but we do not know if others exist. [¹⁸F]DFA accumulation is attenuated in several mouse models of metabolic syndrome, suggesting an association between ribose salvage and glucose and lipid metabolism. These results describe a tool for studying ribose salvage and suggest that plasma ribose is preferentially metabolized in the liver.

molecular imaging | sugar metabolism | Slc2a2

Ribose is a naturally occurring monosaccharide whose metabolites contribute to DNA, RNA, and energy production (1). Most studies and textbooks focus on the intracellular synthesis of ribose-5-phosphate from glucose via the oxidative and nonoxidative pentose phosphate pathways (1) (Fig. 1A). However, a few studies suggest that cells can also salvage extracellular ribose for further intracellular metabolism (2). Ribose is likely the second most abundant carbohydrate in blood, being present at ~100 μM in human fasting serum (3). Ribose is also present in the diet and is absorbed through the intestines into the blood stream (3–5). However, despite the abundance of blood ribose, little is known about ribose salvage, including its biodistribution and regulation.

During salvage, ribose is transported across the cell membrane and phosphorylated by ribokinase (RBKS) to ribose-5-phosphate (6). Ribose-5-phosphate can be incorporated into nucleic acids via the de novo nucleotide synthesis pathway or metabolized to glycolytic intermediates via the nonoxidative pentose phosphate pathway (1). Enzymes in the nonoxidative pentose phosphate pathway include transketolase (TKT) and transaldolase 1 (TALDO1), sequential enzymes that transfer carbons between phosphorylated carbohydrate intermediates. An additional enzyme in the nonoxidative pentose phosphate pathway is ribose-5-phosphate isomerase (RPIA), which catalyzes the interconversion of ribose-5-phosphate and ribulose-5-phosphate (1). Alternatively, the first step to incorporate ribose-5-phosphate into nucleic acids is phosphorylation by phosphoribosyl pyrophosphate synthetase 1 or 2 (PRPS1 or PRPS2) (1) (Fig. 1A).

Several lines of evidence suggest that blood ribose and ribose salvage could be linked to glucose metabolism. Cells interconvert ribose-5-phosphate and glucose-6-phosphate via the non-oxidative pentose phosphate pathway (1). Ribose is metabolized to glucose and glucose-6-phosphate in liver slices and liver en-

zyme extracts (2, 7). Additionally, fasting serum ribose concentrations (~100 μM) in humans are similar to plasma and serum concentrations of other gluconeogenic substrates, including pyruvate (~50 μM) and glycerol (~100 μM) (8, 9). Finally, the conversion of ribose to glucose requires less energy and reducing power than either pyruvate or glycerol (1).

Other data suggest that ribose may have alternative and distinct roles different from those of glucose in the body. Fasting blood ribose concentrations are ~50-fold lower than blood glucose concentrations (3). With few exceptions, cells and tissues cannot survive with ribose as their sole carbohydrate source (10–12). Additionally, RBKS is substrate-inhibited at ribose concentrations of >0.5 mM, suggesting that cells may limit the amount of ribose they salvage (6).

PET is used for imaging and quantifying changes in whole-body metabolism through the use of radiolabeled substrates (13). The potential utility of new PET probes is best exemplified by the radiolabeled glucose analog [¹⁸F]-2-fluoro-2-deoxyglucose ([¹⁸F]FDG). [¹⁸F]FDG has been extensively used both preclinically and clinically to study glucose metabolism in vivo, including to identify metabolic changes during brain development, to monitor myocardial viability, and to image and identify tumors in vivo (13–15). We reasoned that a PET probe for measuring and imaging ribose salvage could provide unique and novel information on this understudied pathway in vivo.

Significance

The saccharide ribose is naturally present in food and circulates in the blood. Previous studies suggest that cells internalize ribose directly from the extracellular space, but how, why, and where this occurs in the body are not well understood. Here, we developed a new PET probe to monitor this process in vivo. Using this probe and [¹⁴C]ribose, we show that ribose salvage is concentrated in the liver. We identify that solute carrier family 2, member 2 is one of potentially several ribose transporters. We demonstrate that ribose salvage is down-regulated during metabolic syndrome. This work raises the possibility that ribose is an important sugar for whole-body metabolism.

Author contributions: P.M.C., G.F., N.M.E., F.O., S.W.B., K.F.F., M.E.P., M.E.J., and O.N.W. designed research; P.M.C., G.F., N.M.E., M.N.M., T.C., E.N.-G., and F.O. performed research; P.M.C., G.F., and N.M.E. contributed new reagents/analytic tools; P.M.C., G.F., N.M.E., M.N.M., T.C., K.F.F., M.E.P., M.E.J., and O.N.W. analyzed data; and P.M.C. and O.N.W. wrote the paper.

Conflict of interest statement: P.M.C., G.F., N.M.E., M.E.J., and O.N.W. are coauthors on a patent application that covers the PET probe described in this paper.

Freely available online through the PNAS open access option.

¹To whom correspondence may be addressed. Email: pclark@mednet.ucla.edu, mphelps@mednet.ucla.edu, or owenwitte@mednet.ucla.edu.

This article contains supporting information online at www.pnas.org/lookup/suppl/doi:10.1073/pnas.1410326111/-DCSupplemental.

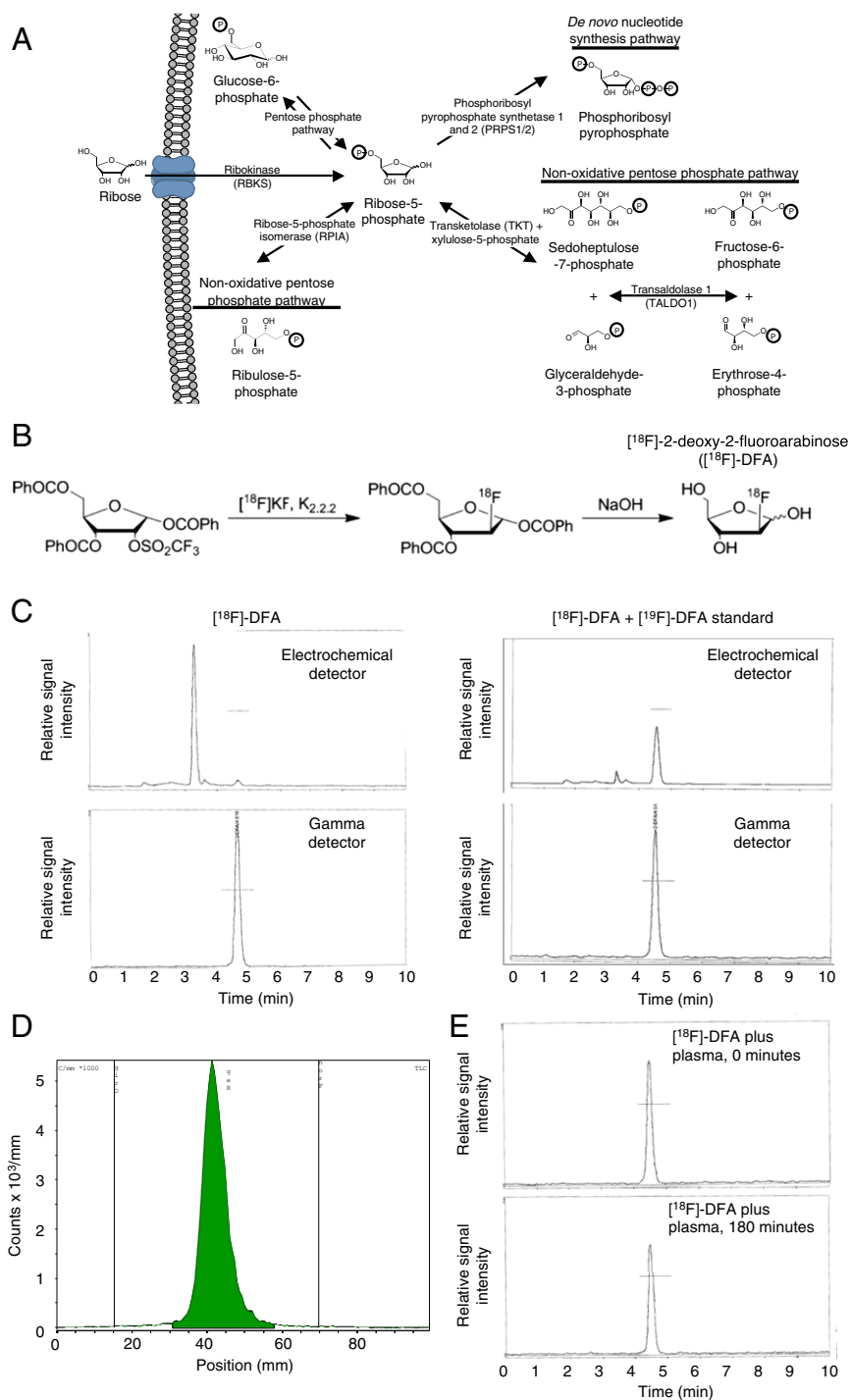


Fig. 1. $[^{18}\text{F}]$ DFA can be prepared in 99% radiochemical purity. (A) Ribose salvage and metabolic pathway. (B) $[^{18}\text{F}]$ DFA synthetic scheme. (C) HPLC analysis of $[^{18}\text{F}]$ DFA with and without $[^{19}\text{F}]$ DFA standard coinjection. In all cases, the signal is normalized to the maximum signal in each chromatogram. (D) Radio-TLC analysis of $[^{18}\text{F}]$ DFA. (E) Radio-HPLC analysis of $[^{18}\text{F}]$ DFA incubated in plasma for 0 and 180 min.

Here, we report and validate a ribose-based PET probe, $[^{18}\text{F}]$ 2-deoxy-2-fluoroarabinose ($[^{18}\text{F}]$ DFA), for studying ribose salvage. Using this probe, we show that ribose salvage is concentrated in the liver. We also demonstrate that solute carrier family 2, member 2 (Slc2a2) is one among potentially several ribose transporters. Finally, we show that ribose salvage is attenuated in mouse models of metabolic syndrome. Our studies suggest that $[^{18}\text{F}]$ DFA is a powerful imaging probe for studying ribose salvage in mice and potentially humans.

Results

$[^{18}\text{F}]$ DFA Is a PET Probe for Ribose Salvage. To understand ribose salvage *in vivo* better, we developed a PET probe that mimics the structure of ribose. An earlier study showed that human RBKS can metabolize ribose and, with lower affinity, arabinose (6). This suggested to us that ribose derivatized at the 2-position with a positron-emitting nuclide could be metabolized through the ribose salvage pathway. Given the clinical success of $[^{18}\text{F}]$ FDG and other $[^{18}\text{F}]$ -fluorinated PET probes, we focused on

[¹⁸F]-fluorinated molecules and reasoned that [¹⁸F]2-deoxy-2-fluororibose ([¹⁸F]DFR) and its epimer, [¹⁸F]DFA, could function as PET probes for measuring the ribose salvage pathway. [¹⁸F]DFR proved challenging to synthesize, so we first studied [¹⁸F]DFA. We fluorinated 2-*O*-(trifluoromethylsulfonyl)-1,3,5-tri-*O*-benzoyl-*D*-ribofuranose with [¹⁸F]F[−] and deprotected with NaOH to yield [¹⁸F]DFA at a 45 ± 1.6% decay-corrected radiochemical yield and 99 ± 0% radiochemical purity, as measured by radio-HPLC and radio-TLC (Fig. 1 *B–D*). [¹⁸F]DFA coeluted with a [¹⁹F]DFA standard on HPLC, suggesting that [¹⁸F]DFA was correctly prepared (Fig. 1*C*). [¹⁸F]DFA has a specific activity of 114.8 ± 32.2 Ci/mmol and is stable in mouse plasma for up to 2 h (Fig. 1*E*).

It is possible that ribose salvage could mirror glucose consumption and that ribose would accumulate preferentially in the heart and brain. Alternatively, one study using light microscopy radioautography with [³H]ribose suggests a wider distribution of ribose salvage with some preference for certain cell types, including hepatocytes, adrenal cortex cells, and cells of the spleen (16). Instead, we found that [¹⁸F]DFA accumulation does not simply reflect glucose consumption and has a unique and specific distribution. PET/computed tomography (CT) images and ex vivo biodistribution studies of mice i.v. injected with [¹⁸F]DFA demonstrated [¹⁸F]DFA accumulation in all organs, with greater accumulation in the liver, kidneys, and intestines than in the heart or brain after 1 h (Fig. 2 *A* and *B*). Additionally, quantification of the [¹⁸F] signal from the time of injection until 3 h postinjection demonstrated that [¹⁸F]DFA accumulated in the liver within 10 min and persisted there throughout the remaining 3 h (Fig. 2*C*). Notably, [¹⁸F]DFA accumulation has a distinctly different biodistribution than glucose consumption, as measured by [¹⁸F]FDG PET imaging (Fig. 2*D*). If DFA accurately mimics ribose in vivo, then our results suggest an underappreciated tissue specificity of whole-body ribose metabolism.

DFA differs from ribose structurally by the replacement of the 2-hydroxyl of ribose with the positron-emitting nuclide [¹⁸F]fluorine and by epimerization at this stereocenter. This replacement could block enzymes in the ribose salvage pathway from metabolizing DFA and potentially cause mislocalization of DFA to organs independent of their ribose salvage activity. Thus, we tested whether DFA mimics ribose in vivo. Mice injected with [¹⁴C]ribose show strong [¹⁴C]ribose accumulation in the liver, kidneys, and intestines after 1 h, as measured by whole-body autoradiography and ex vivo biodistribution experiments (Fig. 2 *E* and *F*). The biodistribution of [¹⁴C]ribose strongly mirrors the biodistribution of [¹⁸F]DFA, except that [¹⁸F]DFA has higher renal and lower blood accumulation than [¹⁴C]ribose. This may suggest that [¹⁸F]DFA clears from the blood into the kidneys faster than ribose. Hepatocytes comprise 60–70% of the cells in the liver, with Kupffer, stellate, and endothelial cells making up the majority of the remainder (17, 18). An earlier study in which rats were i.v. injected with [³H]ribose and radioautography was performed on liver sections suggests that hepatocytes, and not Kupffer cells, salvage the majority of ribose (16). To identify the liver cell types responsible for ribose salvage more carefully, we isolated hepatocytes, Kupffer cells, stellate cells, and endothelial cells and measured ribose accumulation in each preparation. Hepatocytes accumulate 30-fold more ribose than Kupffer, stellate, or endothelial cells (190 ± 18 fmol of ribose per 50,000 hepatocytes vs. 6 ± 1 fmol of ribose per 50,000 Kupffer cells, 6 ± 1 fmol of ribose per 50,000 stellate cells, and 5 ± 1 fmol of ribose per 50,000 endothelial cells) (Fig. 2*G*). This suggests that hepatocytes are the major hepatic cell type to salvage ribose. Coinjection of [¹⁸F]DFA with 25 μmol of ribose diminished [¹⁸F]DFA accumulation in the liver from 9.6 ± 0.9% injected dose per gram (%ID/g) to 4.2 ± 0.8%ID/g (Fig. 2*H*), suggesting that [¹⁸F]DFA and ribose compete for a saturable accumulation

pathway. Finally, we reasoned that if the liver were simply clearing circulating [¹⁸F]DFA, then the level of [¹⁸F]DFA accumulation would be independent of the chirality of the molecule. Mice injected with [¹⁸F]-*L*-2-deoxy-2-fluoroarabinose, an enantiomer of [¹⁸F]DFA, accumulate only 1.3 ± 0.5%ID/g of [¹⁸F]-*L*-2-deoxy-2-fluoroarabinose in the liver compared with 10.2 ± 0.6%ID/g hepatic accumulation when mice were injected with the correct *D* isomer [¹⁸F]DFA (Fig. 2 *B* and *I*). These data suggest that the majority of the hepatic [¹⁸F]DFA signal is from specific accumulation in hepatocytes. Collectively, our data suggest that even though [¹⁸F]DFA differs structurally from ribose through both epimerization and fluorination of the 2-position, [¹⁸F]DFA is an effective mimic for imaging the ribose salvage pathway in vivo.

DFA Is Phosphorylated by RBKS and Further Metabolized by TKT. One advantage of FDG as a PET imaging probe is that FDG is trapped in cells as FDG-6-phosphate and is not further metabolized (13). To understand the properties of DFA as a PET imaging probe better, we studied its metabolism in vitro and in vivo using liquid chromatography/tandem MS (LC/MS/MS) with multiple reaction monitoring (MRM). Human RBKS, TKT, TALDO1, RPIA, PRPS1, and PRPS2, expressed in and isolated from *Escherichia coli* (*SI Materials and Methods*), correctly metabolized their natural substrates (Figs. *S1* and *S2*). We then tested these enzymes on DFA and its metabolites. RBKS metabolized DFA to DFA-5-phosphate, and TKT further metabolized DFA-5-phosphate to 4-deoxy-4-fluorosedoheptulose-7-phosphate (Fig. 3 *A* and *B* and full chromatograms in Fig. *S3*). TALDO1, which would normally metabolize the product of the TKT reaction, requires a 4-hydroxyl group on its substrate and did not metabolize 4-deoxy-4-fluorosedoheptulose-7-phosphate (Fig. 3*C*). Similarly, RPIA normally metabolizes ribose-5-phosphate but requires a 2-hydroxyl on its substrate and did not metabolize DFA-5-phosphate (Fig. 3*D*). Neither PRPS1 nor PRPS2 phosphorylated DFA-5-phosphate to its triphosphate form (Fig. 3*E* and full chromatograms in Fig. *S3*). Our in vitro analyses suggest that DFA is metabolized to DFA-5-phosphate and 4-deoxy-4-fluorosedoheptulose-7-phosphate.

Although we identified that RBKS and TKT metabolize DFA in vitro, the levels and activity of each enzyme in vivo could affect the kinetics of DFA metabolism. To investigate the metabolism of DFA in vivo, we injected mice with 12.5 μmol of DFA; extracted tissue metabolites after 30 min, 1 h, and 3 h; and analyzed these metabolites by LC/MS/MS-MRM. Confirming our in vitro metabolite studies and consistent with our [¹⁸F]DFA biodistribution results, we identified DFA-5-phosphate and 4-deoxy-4-fluorosedoheptulose-7-phosphate but not triphosphorylated DFA in all tissues analyzed (Fig. 3*F* and full chromatograms in Fig. *S4*). Both of these metabolites were present at 30 and 60 min but were lower in abundance or not detectable by 3 h postinjection in all of the tissues analyzed (Fig. *S5*). This suggests either an unidentified metabolic pathway for these molecules or nonspecific clearance of these metabolites, which occurs 1–3 h postinjection. We failed to identify DFA metabolites in the plasma (Fig. 3*G*), suggesting that both DFA-5-phosphate and 4-deoxy-4-fluorosedoheptulose-7-phosphate are trapped in cells. Thus, DFA is metabolized to DFA-5-phosphate and 4-deoxy-4-fluorosedoheptulose-7-phosphate in vivo. Because both of these molecules are charged and not found in plasma, this suggests a potential trapping mechanism for intracellular probe accumulation. Additionally, these data may suggest that the ribose salvage pathway is promiscuous in its substrate specificity, metabolizing ribose as well as a fluorinated derivative of arabinose.

Slc2a2 Can Transport Ribose. A major deficit in our understanding of the ribose salvage pathway is that we do not know which

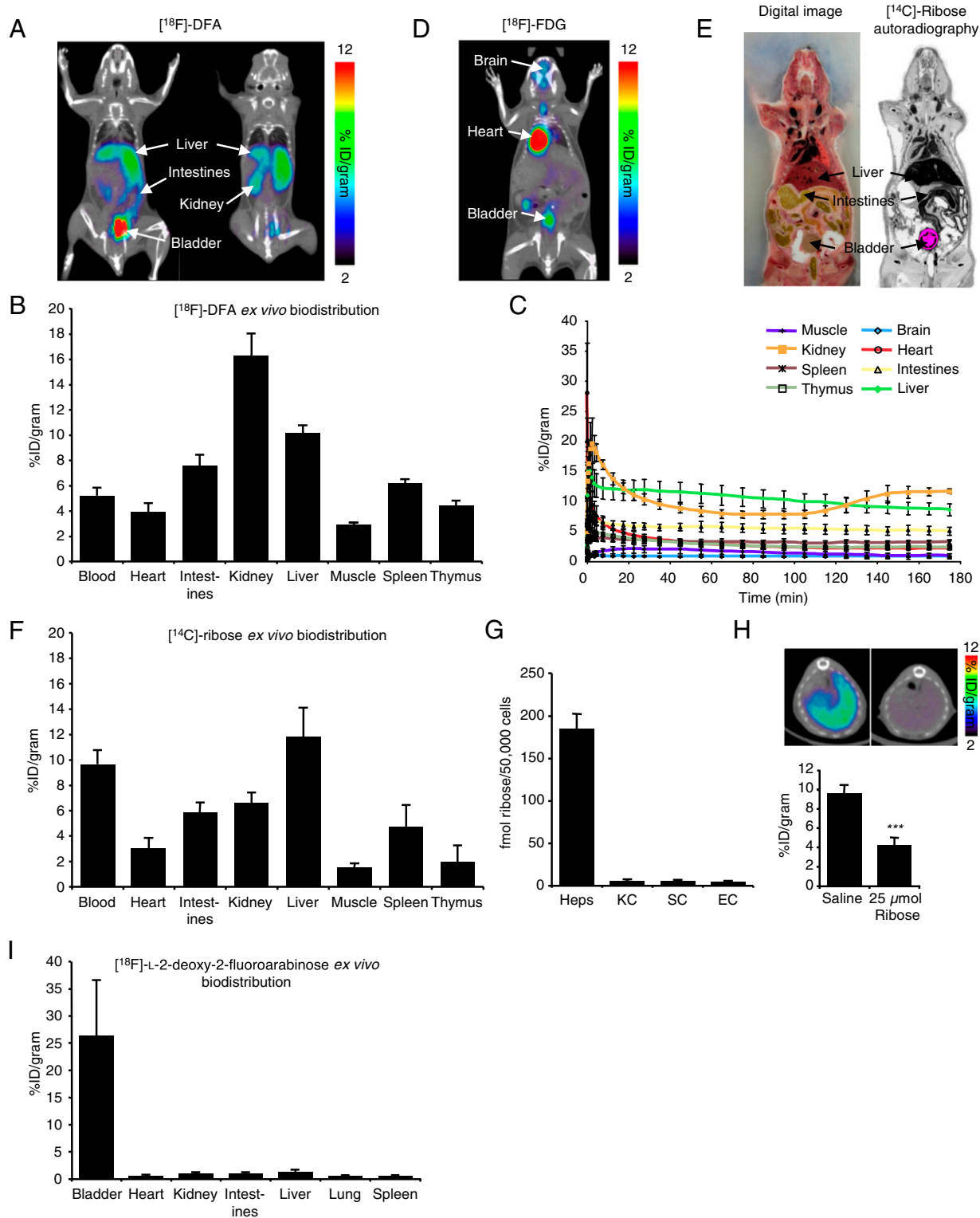


Fig. 2. $[^{18}\text{F}]$ DFA is a PET probe for ribose salvage. (A) Coronal PET/CT image of a mouse i.v. injected with $[^{18}\text{F}]$ DFA. (B) Ex vivo biodistribution of $[^{18}\text{F}]$ DFA. (C) Time activity curves of $[^{18}\text{F}]$ DFA accumulation in several organs from immediately to 3 h postinjection. (D) Coronal PET/CT image of a mouse i.v. injected with $[^{18}\text{F}]$ FDG. (E) Autoradiography image of a mouse 1 h after i.v. injection with $[^{14}\text{C}]$ ribose. (F) Ex vivo biodistribution of $[^{14}\text{C}]$ ribose. (G) Ribose accumulation in isolated and cultured hepatocytes (Heps), Kupffer cells (KC), stellate cells (SC), and endothelial cells (EC). (H) Transverse PET/CT images of mice i.v. injected with $[^{18}\text{F}]$ DFA and saline or $[^{18}\text{F}]$ DFA and 25 μmol of ribose. (I) Ex vivo biodistribution of $[^{18}\text{F}]$ -L-2-deoxy-2-fluoroarabinose. PET images in this and subsequent figures were acquired over 10 min at 1 h postinjection of the PET probe. Ex vivo biodistribution studies were performed 60–70 min postinjection of the radiolabeled probe. Graphs in this and subsequent figures represent mean \pm SEM. Statistical analyses were performed using the Student *t* test. ****P* < 0.001. PET/CT images in this and subsequent figures are representative of three to six independent experiments.

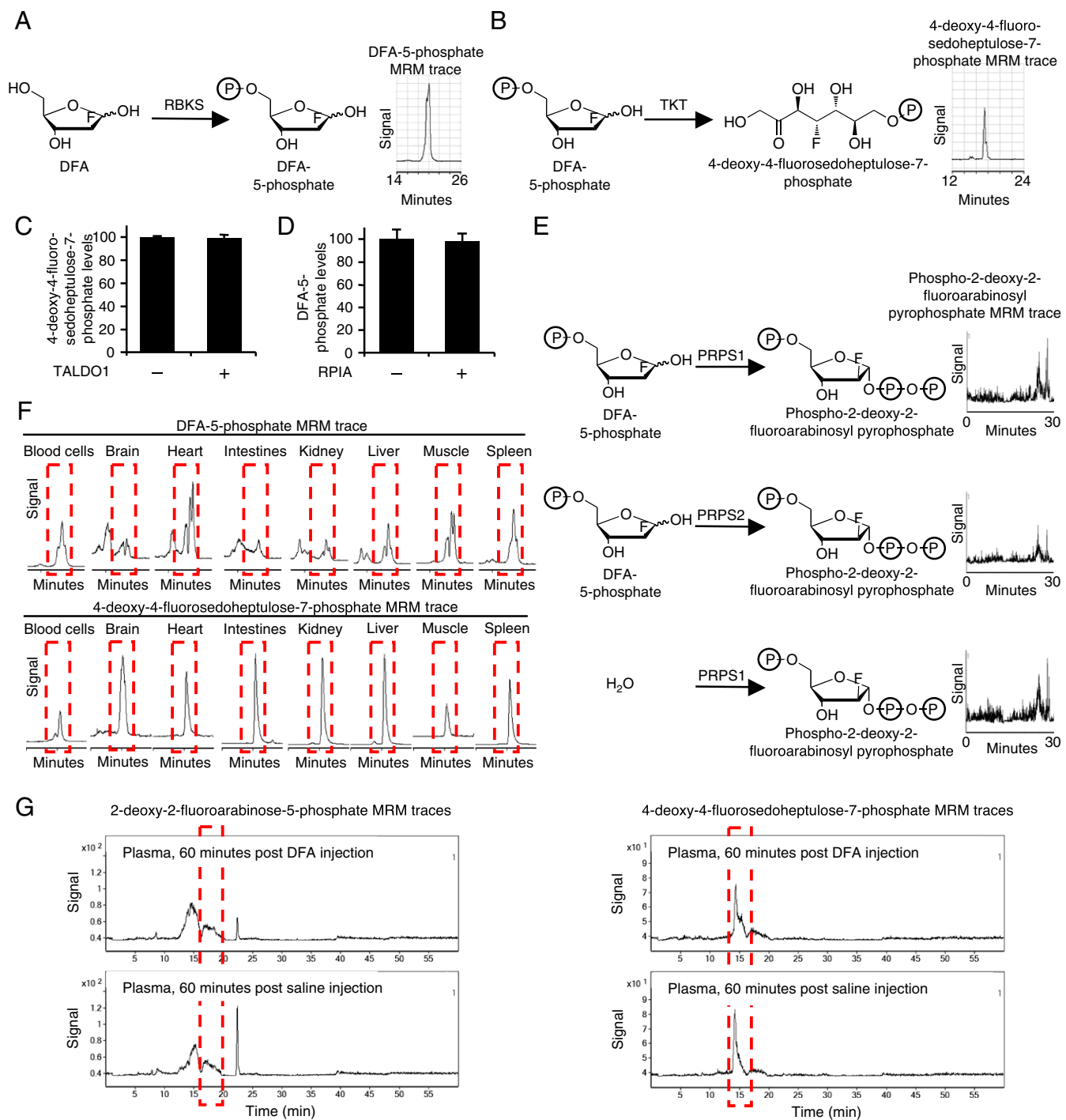


Fig. 3. DFA is phosphorylated by RBKS and further metabolized by TKT. (A) LC/MS/MS-MRM trace of an in vitro reaction between DFA and RBKS [m/z 231 ($M - H$) $^- \rightarrow m/z$ 79]. H, hydrogen; M, molecule. (B) LC/MS/MS-MRM trace of an in vitro reaction between DFA-5-phosphate and TKT [m/z 291 ($M - H$) $^- \rightarrow m/z$ 79]. (C) Relative 4-deoxy-4-fluoro-sedoheptulose-7-phosphate levels in reactions treated with vehicle or TALDO1. (D) Relative DFA-5-phosphate levels in reactions treated with vehicle or RPIA. (E) LC/MS/MS-MRM traces of in vitro reactions between DFA-5-phosphate or water and PRPS1 or PRPS2 [m/z 390.9 ($M - H$) $^- \rightarrow m/z$ 158.9]. (F) LC/MS/MS-MRM traces of DFA metabolites in tissues of mice treated with DFA [DFA-5-phosphate: m/z 231 ($M - H$) $^- \rightarrow m/z$ 79; 4-deoxy-4-fluoro-sedoheptulose-7-phosphate: m/z 291 ($M - H$) $^- \rightarrow m/z$ 97 except for the brain sample, where m/z 291 ($M - H$) $^- \rightarrow m/z$ 79]. Dotted red lines represent the expected elution time for each predicted metabolite. (G) LC/MS/MS-MRM traces of DFA metabolites in plasma of mice treated with saline or DFA [DFA-5-phosphate: m/z 231 ($M - H$) $^- \rightarrow m/z$ 79; 4-deoxy-4-fluoro-sedoheptulose-7-phosphate: m/z 291 ($M - H$) $^- \rightarrow m/z$ 79]. LC/MS/MS-MRM spectra in this and subsequent figures represent the MRM trace for the reaction product. All reactions were performed at least three independent times, and representative traces are presented.

protein or proteins transport ribose into cells. Our [^{18}F]DFA PET images, [^{14}C]ribose autoradiography images, and ex vivo biodistribution studies all suggest that ribose strongly accumu-

lates in the liver with additional accumulation in the intestines and kidneys (Fig. 2 A–C, E, and F). RBKS mRNA levels do not correlate well with [^{14}C]ribose biodistribution in tissues or

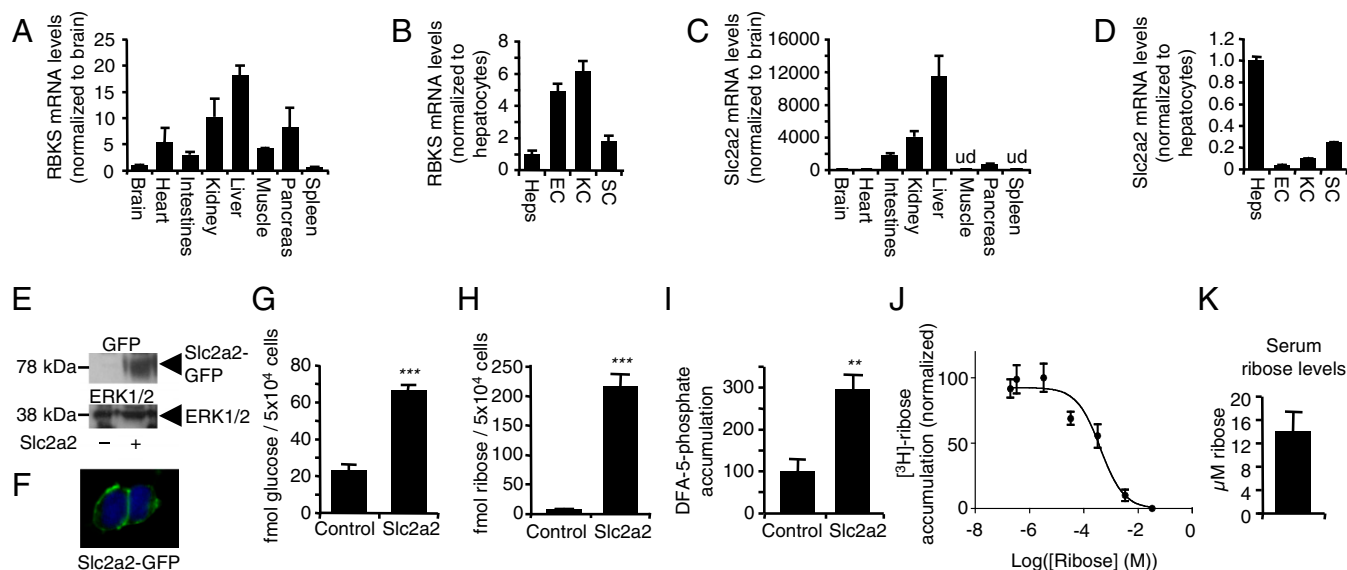


Fig. 4. Slc2a2 can transport ribose. (A) RBKS mRNA levels in mouse tissues. (B) RBKS mRNA levels in isolated and cultured mouse hepatocytes (Heps), endothelial cells (EC), Kupffer cells (KC), and stellate cells (SC). (C) Slc2a2 mRNA levels in mouse tissues. ud, undetectable. (D) Slc2a2 mRNA levels in isolated and cultured mouse Heps, EC, KC, and SC. (E) Immunoblot of cells transfected with a control plasmid or a plasmid expressing Slc2a2-GFP. (F) Confocal microscopy of cells transfected with a plasmid expressing Slc2a2-GFP. (G) [3 H]glucose accumulation in cells transfected with a control plasmid or a plasmid expressing Slc2a2-GFP. (H) [3 H]ribose accumulation in cells transfected with a control plasmid or a plasmid expressing Slc2a2-GFP. (I) Normalized DFA-5-phosphate accumulation in cells transfected with a control plasmid or a plasmid expressing Slc2a2-GFP. (J) Kinetics of ribose transport by Slc2a2. (K) Ad libitum-fed mouse serum ribose levels. ** $P < 0.01$; *** $P < 0.001$.

[3 H]ribose accumulation in isolated liver cells (Fig. 4A and B). This suggests that the ribose transporter may play an important role in defining the biodistribution of ribose accumulation and that the ribose transporter should be expressed more highly in the liver, kidneys, and intestines relative to other tissues, such as the heart. An earlier study indicates that Cytochalasin B, a promiscuous small-molecule ligand that binds to and blocks glucose transport through the Slc2a family of glucose transporters (19), blocks ribose salvage in cultured mammalian cells (20). The best-studied hepatic Slc2a transporter is Slc2a2 (also known as GLUT2) (21). In agreement with previous reports (22), we found that Slc2a2 mRNA levels are enriched in the liver, kidneys, and intestines (Fig. 4C). Additionally, Slc2a2 mRNA levels are 27.3 ± 3.7 -fold, 10.0 ± 1.5 -fold, and 4.1 ± 0.5 -fold higher in hepatocytes than in endothelial, Kupffer, or stellate cells, respectively (Fig. 4D). We hypothesized that Slc2a2 might be a ribose transporter.

To determine whether Slc2a2 transports ribose, we overexpressed a mouse Slc2a2-GFP fusion in 293T cells (Fig. 4E). Overexpressed Slc2a2 localized to the cell surface and increased glucose accumulation from 23.2 ± 3.09 fmol per 5×10^4 cells to 66.4 ± 2.82 fmol per 5×10^4 cells (Fig. 4F and G), indicating correct Slc2a2 function in our system. Slc2a2 overexpression also increased ribose accumulation from 4.10 ± 1.10 fmol per 5×10^4 cells to 215.79 ± 21.81 fmol per 5×10^4 cells and DFA-5-phosphate levels by $300 \pm 60\%$ (Fig. 4H and I). The difference in magnitude between ribose and DFA accumulation caused by Slc2a2 overexpression likely represents differences in the affinity of Slc2a2 for ribose and DFA, although the disparity could be the result of additional ribose or DFA transporters. We measured the apparent $K_{0.5}$ of mouse Slc2a2 for ribose to be $410 \mu\text{M}$ (95% confidence interval: 170–960 μM) (Fig. 4J). Ad libitum-fed mouse serum ribose levels are $14.1 \pm 3.2 \mu\text{M}$ (Fig. 4K). This suggests that Slc2a2 is a low-affinity ribose transporter at physiological blood ribose levels. Notably, these studies neither prove nor imply that Slc2a2 is a major ribose transporter. Additional studies will be required to quantify the precise contribution of Slc2a2 to cellular ribose accumulation.

[18 F]DFA Imaging Suggests That Hepatic Ribose Salvage Is Dysregulated During Metabolic Syndrome. PET imaging allows for rapid and quantitative analyses of biochemical pathways across different physiological and disease states (13). We hypothesized that pathological changes in whole-body metabolism could affect ribose salvage. Because ribose and glucose are connected via intracellular metabolism (1) and also share a transporter (Fig. 4G and H), we focused on models with known alterations in glucose metabolism. We investigated one acute and three chronic mouse models of type I (insulin-dependent) diabetes and metabolic syndrome. The small molecule streptozotocin (STZ) is a pancreatic beta-cell toxin that causes an acute insulin-dependent diabetic phenotype in mice, including hyperglycemia and hypoinsulinemia, within 72 h of treatment (23). STZ treatment increased mouse blood glucose levels from 270 ± 9 mg/dL to 567 ± 19 mg/dL and decreased insulin levels from 1.89 ± 0.78 ng/mL to 0.16 ± 0.03 ng/mL after 5 d but failed to change hepatic [18 F]DFA accumulation (Fig. 5A; control mice: $8.31 \pm 0.56\%$ ID/g, STZ-treated mice: $7.98 \pm 0.19\%$ ID/g).

Mice with genetic KO of the leptin protein (*ob/ob* mice), mice with ectopic expression of the Agouti protein (*A^{y/a}* mice), and mice fed a diet composed of 60% fat (diet-induced obesity mice) are all models of metabolic syndrome characterized by obesity, hyperglycemia, insulin resistance, excess hepatic fat accumulation, and enhanced hepatic lipogenesis (24–28). Traditional gluconeogenic substrates, such as lactate and pyruvate, and ATP levels are similar or slightly higher per gram of tissue in the livers of *ob/ob* mice compared with control mice (29). Additionally, per gram of tissue, livers of *ob/ob* mice have enhanced glucose release but no difference in pyruvate uptake (30, 31). We imaged ribose salvage in all three mouse models at time points when the mice were clearly obese and hyperglycemic (*SI Materials and Methods*) and found a significant decrease in [18 F]DFA accumulation per gram of liver tissue, as measured in a 3-mm 3 region (Fig. 5B; WT mice: $9.99 \pm 0.00\%$ ID/g, *ob/ob* mice: $4.47 \pm 0.16\%$ ID/g; WT mice: $7.72 \pm 0.59\%$ ID/g, *A^{y/a}* mice: $4.65 \pm 0.40\%$ ID/g; control mice: $6.35 \pm 0.32\%$ ID/g; diet-induced obesity mice: $4.35 \pm$

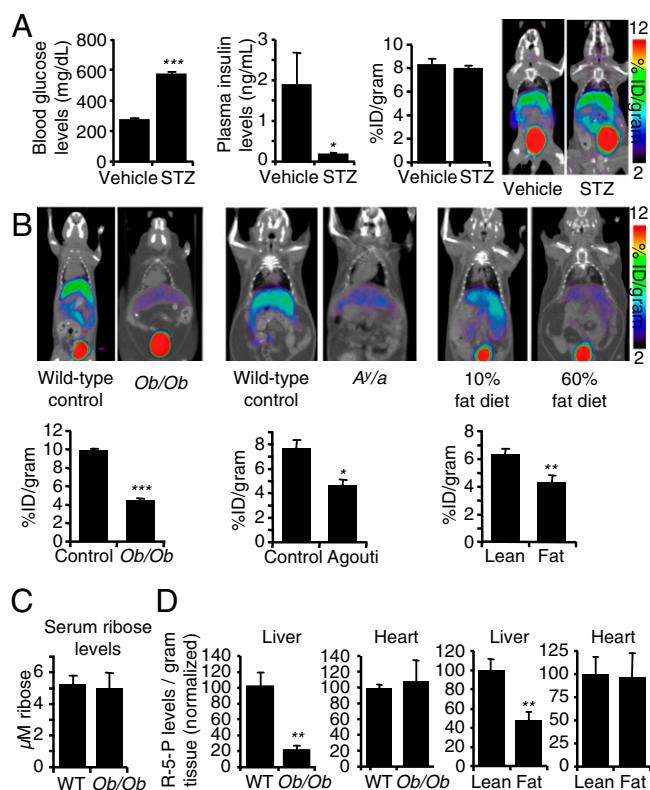


Fig. 5. Ribose salvage is down-regulated in mouse models of metabolic syndrome but not diabetes. (A) Blood glucose levels, plasma insulin levels, and coronal [^{18}F]DFA PET/CT image of mice treated with vehicle or STZ. (B) Coronal [^{18}F]DFA PET/CT images of mouse models of metabolic syndrome. (C) Serum ribose levels in ad libitum-fed WT and *ob/ob* mice. (D) Ribose-5-phosphate (R-5-P) levels in the liver and heart of WT and *ob/ob* mice or mice fed a 10% fat diet (Lean) and mice fed a 60% fat diet (Fat). * $P < 0.05$; ** $P < 0.01$; *** $P < 0.001$.

0.42%ID/g). Serum ribose levels were unaffected in *ob/ob* mice compared with WT mice (Fig. 5C), suggesting that competition between blood ribose and [^{18}F]DFA cannot account for decreased [^{18}F]DFA accumulation. To determine whether decreased [^{18}F]DFA accumulation in these mice was associated with changes in hepatic ribose-5-phosphate levels, we measured ribose-5-phosphate levels using LC/MS/MS-MRM. Ribose-5-phosphate levels, normalized to tissue weight, were $82.3 \pm 3.1\%$ lower in the liver but unchanged in the heart of *ob/ob* mice and $51.9 \pm 8.7\%$ lower in the liver but unchanged in the heart of diet-induced obesity mice (Fig. 5D). This suggests that dysregulated hepatic ribose salvage and ribose metabolism are associated with metabolic syndrome but not type I diabetes.

Discussion

We have developed a PET probe, [^{18}F]DFA, for studying ribose salvage in vivo, and we use this probe to demonstrate that the activity of the ribose salvage pathway is high in the liver, with additional activity in the kidneys and intestines. We provide evidence that the ribose salvage pathway contributes to hepatic [^{18}F]DFA accumulation, although we cannot exclude the possibility that some of the [^{18}F]DFA signal is due to nonspecific accumulation. The protein Slc2a2 transports both ribose and DFA, and Slc2a2 mRNA levels are highly enriched in the liver, kidneys, and intestines. We do not yet know if Slc2a2 is the major ribose transporter in the liver. We identify tissues, such as the muscle and spleen, that salvage ribose but have no detectable Slc2a2 mRNA levels. This suggests the existence of additional ribose transporters.

Ribose salvage occurs in all tissues analyzed, including the heart and brain. Previous studies suggest that exogenous ribose is metabolized to glucose and glucose-6-phosphate in liver protein extracts and liver slices (2, 7). This suggests that the liver uses ribose as a gluconeogenic substrate. Another study suggests that HeLa cells incorporate as much as 85% of exogenous ribose into nucleic acids (12). Thus, different cell types and cancer cells may use the ribose salvage pathway to provide precursors for distinct cellular pathways.

We show that metabolic syndrome but not type I diabetes is associated with altered hepatic ribose salvage. Metabolic syndrome is a complex disease that includes disorders like obesity, insulin resistance, glucose intolerance, and hypertension, with the unifying theme that individuals with metabolic syndrome have an increased risk of atherosclerotic cardiovascular disease (32–34). Metabolic syndrome is also associated with an increased risk of developing type 2 diabetes (35). Here, we show that [^{18}F]DFA accumulation is diminished in several mouse models of metabolic syndrome. The American Heart Association and National Heart, Lung, and Blood Institute suggest that patients be diagnosed with metabolic syndrome if they possess a majority of the following symptoms: elevated waist circumference, elevated triglycerides, reduced HDL-cholesterol, elevated blood pressure, or elevated fasting glucose levels (35). [^{18}F]DFA imaging would not likely rival the use of these simple criteria as a diagnostic tool. However, metabolic syndrome is associated with interrelated and progressive liver pathologies, including nonalcoholic fatty liver disease (NAFL), nonalcoholic steatohepatitis, liver fibrosis, and hepatocellular carcinoma (34). Noninvasively diagnosing and staging NAFL remains a clinical challenge (36, 37). Blood tests for liver function often give a mild phenotype in patients with NAFL, and other liver diseases, such as alcoholic liver disease and autoimmune liver disease, can manifest with similar clinical findings (37). Imaging modalities, such as ultrasound, are only moderately predictive, and invasive liver biopsies remain the preferred method for diagnosing NAFL (37). We do not yet have data to suggest whether changes in [^{18}F]DFA imaging could be used as an early predictor of or to stage NAFL. However, whole-body PET imaging with [^{18}F]DFA may play a role in the future during the diagnosis and staging of NAFL and other liver malignancies.

Additional studies will be required to identify the mechanisms that explain metabolic syndrome-associated changes in hepatic ribose salvage. Physiologically, changes in hepatic lipid levels or inflammation may contribute to lower ribose salvage. Changes in insulin or insulin signaling would be unlikely to play a role, because ribose salvage is unaffected in our model of insulin-dependent diabetes. One possible molecular mechanism includes changes in RBKS activity. Little is known about the regulation of RBKS activity. However, one study suggests that RBKS activity peaks during the S, G₂, and M phases of the cell cycle and can be found in both soluble and membrane-associated protein preparations (38).

It remains to be determined whether changes in ribose salvage contribute to or represent an adaptive response to metabolic syndrome. Our data suggest that the liver is a significant sink for blood ribose. Although we fail to identify changes in serum ribose levels in our model of metabolic syndrome, it remains to be determined whether serum ribose levels are altered in humans with metabolic syndrome. One possibility is that decreased hepatic ribose salvage leads to greater serum ribose levels and enhanced vascular damage. Ribose is greater than 50-fold more efficient than glucose at nonenzymatic glycation of collagen fibers to form advanced glycation end products (AGEs) (39, 40). AGEs have been suggested to contribute to vascular dysfunction and cardiovascular disease (41). Even though human blood ribose levels are ~50-fold lower than blood glucose levels, the dramatically greater propensity of ribose to form AGEs suggests that elevated blood ribose levels could have a significant effect on AGE formation in vivo. Pentosidines are a specific type of

AGE that can form between ribose, lysine, and arginine (42). Metabolic syndrome is a risk factor for diabetes (35). Plasma levels of pentosidines are elevated 2.5-fold in diabetics, and serum pentosidine levels in type II diabetes are positively associated with vascular complications (42, 43). Thus, decreased hepatic ribose salvage could lead to higher blood ribose levels, increased AGE formation, and enhanced vascular damage. Future studies will examine how changes in hepatic ribose salvage affect AGE formation.

Slc2a2 KO mice do not survive past approximately 3 wk of age, but Slc2a2 KO mice with pancreatic overexpression of the glucose transporter Slc2a1 or liver-specific Slc2a2 KO mice are viable (44–46). These mice have impaired glycogen mobilization during fasting, liver hyperplasia, and glucose intolerance (45, 46). Fanconi–Bickel syndrome is an autosomal recessive disorder in humans associated with mutations in Slc2a2 (47). Hepatic phenotypes of patients with Fanconi–Bickel syndrome include hepatomegaly and enhanced glycogen accumulation (48). Slc2a2 is a high-capacity glucose transporter (21), and many phenotypes found in Slc2a2 KO mice and patients with Fanconi–Bickel syndrome are likely caused by altered glucose consumption. However, we show that Slc2a2 also transports ribose. Yeast that lack the homolog of human RBKS show enhanced glycogen accumulation (49), suggesting that ribose salvage may regulate glycogen levels in yeast. This suggests that some of the phenotypes associated with Slc2a2 knockdown or mutations, such as enhanced glycogen accumulation, may be related to limited ribose salvage. These results will have to be interpreted further as future studies determine the precise contribution of Slc2a2 to ribose salvage.

Studies of *in vivo* biochemistry and metabolism will require carefully designed and validated chemical probes. Here, we de-

scribe and validate a novel PET probe, [^{18}F]DFA. Unlike most other types of chemical probes, PET tracers can be used *in vitro*, *in vivo* in mice, and eventually *in vivo* in humans. [^{18}F]DFA is an analog of ribose with limited metabolism that enables precise measurements of the activity of the ribose salvage pathway. We anticipate that [^{18}F]DFA will provide a powerful tool for advancing our understanding of the ribose salvage pathway *in vitro* and *in vivo*.

Materials and Methods

Detailed methods describing [^{18}F]DFA synthesis and characterization, micro-PET/CT imaging, autoradiography, quantitative reverse transcription PCR, transporter studies, LC/MS/MS-MRM, immunoblotting, and plasma ribose level measurements can be found in the *SI Materials and Methods*.

All data represent the mean \pm SEM. Statistical analyses were performed using the Student *t* test in Microsoft Excel. Graphs were created in Microsoft Excel or GraphPad Prism.

ACKNOWLEDGMENTS. We thank Dr. David Stout, members of the Crump Institute for Molecular Imaging, and members of the Pasarow Mass Spectrometry Laboratory for their technical assistance and advice. We also thank Drs. Jessica Rexach, Steven Bensinger, Peter Tontonoz, Peter Edwards, Alan Saltiel, and Gerald Schulman, as well as members of the laboratory of O.N.W., for providing useful critiques of this work. We thank Mireille Riedinger for cloning the Slc2a2 construct. We thank Ralph and Marjorie Crump for a donation made to the University of California, Los Angeles (UCLA) Crump Institute for Molecular Imaging. P.M.C. and M.N.M. are supported by the California Institute of Regenerative Medicine Training Grant TG2-01169. P.M.C. is also supported by the UCLA Scholars in Oncologic Molecular Imaging Program, National Cancer Institute Grant R25T CA098010, and UCLA *In Vivo* Cellular and Molecular Imaging Center Career Development Award P50 CA086306. O.N.W. is an Investigator of the Howard Hughes Medical Institute and is partially supported by the Eli and Edythe Broad Center of Regenerative Medicine and Stem Cell Research.

- Berg JM, Tymoczko JL, Stryer L (2002) *Biochemistry* (Freeman, New York).
- Katz J, Abraham S, Hill R, Chaikoff IL (1955) The occurrence and mechanism of the hexose monophosphate shunt in rat liver slices. *J Biol Chem* 214(2):853–868.
- Gross M, Zöllner N (1991) Serum levels of glucose, insulin, and C-peptide during long-term D-ribose administration in man. *Klin Wochenschr* 69(1):31–36.
- Sanchez-Mata MC, Penuela-Teruel MJ, Camara-Hurtado M, Diez-Marques C, Torrijas-Me ME (1998) Determination of mono-, di-, and oligosaccharides in legumes by high-performance liquid chromatography using an amino-bonded silica column. *J Agric Food Chem* 46(9):3648–3652.
- Naito Y (1944) Biochemical studies on d-Ribose, with special reference to the mechanism of absorption of sugars from intestinal tract. *J Biochem* 36(1):131–161.
- Park J, van Koeveerdin P, Singh B, Gupta RS (2007) Identification and characterization of human ribokinase and comparison of its properties with *E. coli* ribokinase and human adenosine kinase. *FEBS Lett* 581(17):3211–3216.
- Williams JF, Clark MG, Blackmore PF (1978) The fate of ^{14}C in glucose 6-phosphate synthesized from [^{14}C]ribose 5-phosphate by enzymes of rat liver. *Biochem J* 176(1):241–256.
- Doar JW, Wynn V, Cramp DG (1968) Blood pyruvate and plasma glucose levels during oral and intravenous glucose tolerance tests in obese and non-obese women. *Metabolism* 17(8):690–701.
- Jellum E, Björnstad P (1964) Quantitative gas-liquid chromatographic determination of free glycerol in blood serum. *J Lipid Res* 5(3):314–317.
- Mahoney JR, Jr, Sako EY, Seymour KM, Marquardt CA, Foker JE (1989) A comparison of different carbohydrates as substrates for the isolated working heart. *J Surg Res* 47(6):530–534.
- Chang RS (1960) Genetic study of human cells *in vitro*. Carbohydrate variants from cultures of HeLa and conjunctival cells. *J Exp Med* 111(2):235–254.
- Reitzer LJ, Wice BM, Kennell D (1980) The pentose cycle. Control and essential function in HeLa cell nucleic acid synthesis. *J Biol Chem* 255(12):5616–5626.
- Phelps ME (2000) Positron emission tomography provides molecular imaging of biological processes. *Proc Natl Acad Sci USA* 97(16):9226–9233.
- Tillisch J, et al. (1986) Reversibility of cardiac wall-motion abnormalities predicted by positron tomography. *N Engl J Med* 314(14):884–888.
- Chugani HT, Phelps ME, Mazziotta JC (1987) Positron emission tomography study of human brain functional development. *Ann Neurol* 22(4):487–497.
- Gonçalves RP, Bennett GC, Leblond CP (1969) Fate of ^3H -ribose in the rat as detected by radioautography. *Anat Rec* 165(4):543–557.
- Malarkey DE, Johnson K, Ryan L, Boorman G, Maronpot RR (2005) New insights into functional aspects of liver morphology. *Toxicol Pathol* 33(1):27–34.
- Alpini G, Phillips JO, Vroman B, LaRusso NF (1994) Recent advances in the isolation of liver cells. *Hepatology* 20(2):494–514.
- Ciaraldi TP, Horuk R, Matthaei S (1986) Biochemical and functional characterization of the rat liver glucose-transport system. Comparisons with the adipocyte glucose-transport system. *Biochem J* 240(1):115–123.
- Lager I, Fehr M, Frommer WB, Lalonde S (2003) Development of a fluorescent nanosensor for ribose. *FEBS Lett* 553(1–2):85–89.
- Zhao FQ, Keating AF (2007) Functional properties and genomics of glucose transporters. *Curr Genomics* 8(2):113–128.
- Thorens B, Sarkar HK, Kaback HR, Lodish HF (1988) Cloning and functional expression in bacteria of a novel glucose transporter present in liver, intestine, kidney, and beta-pancreatic islet cells. *Cell* 55(2):281–290.
- Hayashi K, Kojima R, Ito M (2006) Strain differences in the diabetogenic activity of streptozotocin in mice. *Biol Pharm Bull* 29(6):1110–1119.
- Iwatsuka H, Shino A, Suzuki Z (1970) General survey of diabetic features of yellow KK mice. *Endocrinol Jpn* 17(1):23–35.
- Gallou-Kabani C, et al. (2007) C57BL/6J and AJ mice fed a high-fat diet delineate components of metabolic syndrome. *Obesity (Silver Spring)* 15(8):1996–2005.
- Shimomura I, Bashmakov Y, Horton JD (1999) Increased levels of nuclear SREBP-1c associated with fatty livers in two mouse models of diabetes mellitus. *J Biol Chem* 274(42):30028–30032.
- Biddinger SB, et al. (2005) Effects of diet and genetic background on sterol regulatory element-binding protein-1c, stearoyl-CoA desaturase 1, and the development of the metabolic syndrome. *Diabetes* 54(5):1314–1323.
- Anstee QM, Goldin RD (2006) Mouse models in non-alcoholic fatty liver disease and steatohepatitis research. *Int J Exp Pathol* 87(1):1–16.
- Elliott J, Hems DA, Beloff-Chain A (1971) Carbohydrate metabolism of the isolated perfused liver of normal and genetically obese—Hyperglycaemic (ob-ob) mice. *Biochem J* 125(3):773–780.
- Elliott J, Dade E, Salmon DM, Hems DA (1974) Hepatic metabolism in normal and genetically obese mice. *Biochim Biophys Acta* 343(2):307–323.
- Assimakopoulos-Jeannet F, Singh A, Le Marchand Y, Loten EG, Jeanrenaud B (1974) Abnormalities in lipogenesis and triglyceride secretion by perfused livers of obese-hyperglycaemic (ob-ob) mice: Relationship with hyperinsulinaemia. *Diabetologia* 10(2):155–162.
- Grundy SM (2008) Metabolic syndrome pandemic. *Arterioscler Thromb Vasc Biol* 28(4):629–636.
- Moller DE, Kaufman KD (2005) Metabolic syndrome: A clinical and molecular perspective. *Annu Rev Med* 56:45–62.
- Watanabe S, Yaginuma R, Ikejima K, Miyazaki A (2008) Liver diseases and metabolic syndrome. *J Gastroenterol* 43(7):509–518.
- Grundy SM, et al.; American Heart Association; National Heart, Lung, and Blood Institute (2005) Diagnosis and management of the metabolic syndrome: An American Heart Association/National Heart, Lung, and Blood Institute Scientific Statement. *Circulation* 112(17):2735–2752.
- Festi D, et al. (2013) Review article: The diagnosis of non-alcoholic fatty liver disease—Availability and accuracy of non-invasive methods. *Aliment Pharmacol Ther* 37(4):392–400.

37. Malnick SD, Beergabel M, Knobler H (2003) Non-alcoholic fatty liver: A common manifestation of a metabolic disorder. *QJM* 96(10):699–709.
38. Jargiello P (1982) Altered expression of ribokinase activity in Novikoff hepatoma variants. *Biochim Biophys Acta* 698(1):78–85.
39. Bailey AJ, Sims TJ, Avery NC, Halligan EP (1995) Non-enzymic glycation of fibrous collagen: Reaction products of glucose and ribose. *Biochem J* 305(Pt 2):385–390.
40. Valencia JV, et al. (2004) Advanced glycation end product ligands for the receptor for advanced glycation end products: Biochemical characterization and formation kinetics. *Anal Biochem* 324(1):68–78.
41. Brownlee M, Cerami A, Vlassara H (1988) Advanced glycosylation end products in tissue and the biochemical basis of diabetic complications. *N Engl J Med* 318(20):1315–1321.
42. Odetti P, Fogarty J, Sell DR, Monnier VM (1992) Chromatographic quantitation of plasma and erythrocyte pentosidine in diabetic and uremic subjects. *Diabetes* 41(2):153–159.
43. Kerkeni M, et al. (2013) Pentosidine as a biomarker for microvascular complications in type 2 diabetic patients. *Diab Vasc Dis Res* 10(3):239–245.
44. Guillam MT, et al. (1997) Early diabetes and abnormal postnatal pancreatic islet development in mice lacking Glut-2. *Nat Genet* 17(3):327–330.
45. Burcelin R, del Carmen Muñoz M, Guillam MT, Thorens B (2000) Liver hyperplasia and paradoxical regulation of glycogen metabolism and glucose-sensitive gene expression in GLUT2-null hepatocytes. Further evidence for the existence of a membrane-based glucose release pathway. *J Biol Chem* 275(15):10930–10936.
46. Seyer P, et al. (2013) Hepatic glucose sensing is required to preserve β cell glucose competence. *J Clin Invest* 123(4):1662–1676.
47. Santer R, et al. (1997) Mutations in GLUT2, the gene for the liver-type glucose transporter, in patients with Fanconi-Bickel syndrome. *Nat Genet* 17(3):324–326.
48. Manz F, et al. (1987) Fanconi-Bickel syndrome. *Pediatr Nephrol* 1(3):509–518.
49. Wilson WA, Wang Z, Roach PJ (2002) Systematic identification of the genes affecting glycogen storage in the yeast *Saccharomyces cerevisiae*: Implication of the vacuole as a determinant of glycogen level. *Mol Cell Proteomics* 1(3):232–242.